Applied Surface Science 389 (2016) 311–315

Contents lists available at ScienceDirect

Applied Surface Science

journal homepage: www.elsevier.com/locate/apsusc

Role of the oxidation state of cerium on the ceria surfaces for silicate adsorption

Jihoon Seo[a,1], Jinok Moon[a,b,1], Joo Hyun Kim[a], Kangchun Lee[a], Junha Hwang[a,c], Heesung Yoon[a], Dong Kee Yi[d,*], Ungyu Paik[a,*]

[a] WCD Department of Energy Engineering, Hanyang University, Seoul, South Korea
[b] Clean/CMP Technology Team, Memory, Samsung Electronics, Hwaseong, South Korea
[c] Materials R&D Center, K.C.Tech, Anseong, South Korea
[d] Department of Chemistry, Myongji University, Yongin, South Korea

ARTICLE INFO

Article history:
Received 11 March 2016
Received in revised form 20 June 2016
Accepted 29 June 2016
Available online 25 July 2016

Keywords:
Ceria
Particle size
Oxidation state
Adsorption isotherm
Silicate ions

ABSTRACT

In this study, we have investigated the role of the Ce oxidation state (Ce^{3+}/Ce^{4+}) on the CeO_2 surfaces for silicate adsorption. In aqueous medium, the Ce^{3+} sites lead to the formation of −OH groups at the CeO_2 surface through H_2O dissociation. Silicate ions can adsorb onto the CeO_2 surface through interaction with the −OH groups (−Ce−OH− + −Si−O$^-$ ↔ −Ce−O−Si− + OH$^-$). As the Ce^{3+} concentration increased from 19.3 to 27.6%, the surface density of −OH group increased from 0.34 to 0.72 OH/nm^2. To evaluate the adsorption behaviors of silicate ions onto CeO_2 NPs, we carried out an adsorption isothermal analysis, and the adsorption isotherm data followed the Freundlich model. The Freundlich constant for the relative adsorption capacity (K_F) and adsorption intensity ($1/n$) indicated that CeO_2 NPs with high Ce^{3+} concentration show higher adsorption affinity with silicate ions. As a result, we have demonstrated that the Ce oxidation state (Ce^{3+}/Ce^{4+}) on the CeO_2 surface can have a significant influence on the silicate adsorption.

1. Introduction

Ceria (CeO_2) nanoparticles (NPs) have been widely used as a promising material in various applications in the fields of catalysis [1], fuel cells [2], gas sensors [3], and chemical mechanical planarization (CMP) [4,5]. In all these applications, the high performance of CeO_2 NPs is attributed to their rich O vacancies and low redox potential [6,7]. It is well known that O vacancies are formed due to the highly mobile nature of the surface oxygens. Two excess electrons, left behind by the formation of O vacancies, are localized on the 4f-state of the nearest Ce ions, leading to a valence change in the Ce ions from Ce^{4+} to Ce^{3+} [8,9].

The Ce^{3+} ions at the surface are active sites for reactions in most applications [6,10,11]. In aqueous medium, Ce^{3+} ions act as active sites for H_2O dissociation, resulting in the formation of −OH groups at the surface [12]. The presence of −OH groups on the CeO_2 surface allows for various interactions (e.g., molecular adsorption, desorption) in their many applications. In CMP applications, the OH groups can form a strong Ce−O−Si−O− bonding with silicate ions (−Ce−OH + −Si−O$^-$ ↔ −Ce−O−Si− + OH$^-$) [13]. The formation of Ce−O−Si bonding directly corresponds with the polishing efficiency of CeO_2 NPs [13]. The high affinity and binding energy with silicate ions lead to an increase in the formation of Ce−O−Si bonding, which can increase the removal rate of SiO_2 films [14–17].

In our previous study, the surface function effects (e.g., −OH, $-NO_3$ groups) on the interaction between CeO_2 and silicate ions were studied through adsorption isotherms and theoretical analyses [15]. Besides the surface functionalities, the surface Ce oxidation state (Ce^{3+}/Ce^{4+}) can have a significant influence on the interactions of CeO_2 NPs with silicate ions. However, there is still a lack of understanding on the role of the Ce oxidation state (Ce^{3+}/Ce^{4+}) in the CeO_2 NPs for the interactions with silicate ions.

Herein, we prepared the CeO_2 NPs at different Ce^{3+} concentrations, and the corresponding adsorption properties of silicate ions onto CeO_2 surfaces were studied. The Ce^{3+} concentration on the surface depends on the size of the CeO_2 NPs. The Ce^{3+} concentration increased with decreasing NP size due to the increase of the surface to volume ratio of the NPs [18–21]. To prepare the CeO_2 NPs at different Ce^{3+} concentration, three different-sized CeO_2 NPs (small, mid, and large CeO_2, hereafter noted as S-CeO_2, M-CeO_2, and L-CeO_2, respectively) were synthesized in supercritical water (SCW) [22]. The adsorption properties of silicate ions onto three different-sized CeO_2 NPs were investigated through adsorption isothermal

* Corresponding authors.
E-mail addresses: vitalis@mju.ac.kr (D.K. Yi), upaik@hanyang.ac.kr (U. Paik).
[1] These authors contributed equally to this work.

http://dx.doi.org/10.1016/j.apsusc.2016.06.193

analysis. Adsorption isotherm data for the silicate ions onto CeO_2 surfaces were fitted using the Langmuir and Freundlich models.

2. Experimental section

2.1. Synthesis of CeO_2 NPs

CeO_2 NPs were synthesized as follows. Precursor solutions: To prepare S-CeO_2 NPs, ammonium cerium nitrate was dissolved at 20.0 wt% in de-ionized water (DIW). To obtain M-CeO_2 and L-CeO_2 NPs, 37.5 wt% cerium nitrate solution was prepared in DIW. SCW: DIW was preheated to 400, 470 and 350 °C for the S-CeO_2, M-CeO_2 and L-CeO_2 NPs, respectively. Precursor solutions and SCW were simultaneously delivered at a rate of 40 and 160 mL min^{-1}, respectively, into the reactor. The reactors were controlled at the same temperature using SCW. The obtained CeO_2 NPs were rapidly and continuously collected. They were filtered, washed and dried in an oven at 100 °C for 12 h. Before the characterization, CeO_2 NPs were further dried at 100 °C in a vacuum oven for 12 h to remove residual water.

2.2. Material characterization

The CeO_2 NPs were characterized using various tools as follows. X-ray diffraction patterns of CeO_2 NPs were estimated using an X-ray diffraction analyzer (XRD, Bruker, New D8 Advance). The specific surface areas were measured by the Brunauer–Emmett–Teller (BET) method using N_2 gas adsorption at 77 K (BET, Quantachrome, Autosorb-1). Electron microscope images were obtained by a transmission electron microscope (TEM, JEOL, JEM-2100F). The average sizes (d_{TEM}) of the CeO_2 NPs were calculated from the TEM images using the ImageJ analysis software (average 200 particles counted). The Ce^{3+} concentrations in CeO_2 NPs were calculated using an X-ray photoelectron spectrometer (XPS, Thermo Fisher Scientific Co., theta probe base system). The surface characteristics of CeO_2 NPs were analyzed using Fourier transform infrared spectroscopy (FT-IR, Nicolet 5700, ThermoElectron) using an attenuated transmission reflectance (ATR, Smart Miracle, Pike Tech.) accessory with a ZnSe crystal. The weight loss of CeO_2 NPs was estimated using a thermo gravimetric analyzer with a mass spectrometer (TGA-MS, SDT Q600, TA Instruments) in the temperature range of 40–600 °C at a ramping rate of 10 °C/min in N_2. It was used to calculate the number of —OH groups per area (#OH/nm^2) of CeO_2 NPs.

2.3. Adsorption isotherm

The adsorption behaviors of silicate ions on the CeO_2 NPs were determined through the solution-depletion method using inductively coupled plasma atomic emission spectroscopy (ICP-AES, Optima 7300 DV, Perkin–Elmer). CeO_2 suspensions were prepared as a function of the silicate ions. The pH was adjusted to 7.0 by the addition of a HNO_3 and NH_4OH solutions. Suspensions were aged for 12 h at room temperature under mixing. Then, they were centrifuged at 30,000 rpm for 20 min to obtain the unabsorbed silicate ions. Their supernatants were filtered using a 0.02 μm Anotop 25 syringe filter, and then measured using ICP. The adsorption isotherms of silicate ions on the CeO_2 NPs were derived from the difference between the added and remaining amount of silicate ions in the supernatants [20].

3. Results and discussion

We prepared three samples (S-CeO_2, M-CeO_2, and L-CeO_2) at different Ce^{3+} concentrations to understand the role of the Ce oxidation state (Ce^{3+}/Ce^{4+}) of CeO_2 NPs for interactions with silicate ions. The particle sizes (d_{BET}) of the CeO_2 NPs were calculated from $d_{BET} = 6000/(SSA_{BET}\,\rho)$, where SSA_{BET} is the specific surface area (m^2/g) and ρ is the density of CeO_2 (7.2 g/cm^3). The resulting d_{BET} values were 11.8 (S-CeO_2), 63.1 (M-CeO_2), and 320.5 nm (L-CeO_2) (Table 1). Fig. 1 shows the XRD patterns of the CeO_2 NPs. All the CeO_2 NPs have a well crystalline cubic fluorite structure (JCPDS 65-5923). The crystallite sizes (d_{XRD}) were calculated using the full-width at half-maximum of the (111) peak from the Scherrer equation, and the lattice parameters were obtained from the (111) diffraction peak position. The d_{XRD} values of the CeO_2 NPs are summarized in Table 1. Fig. 1 (b) shows a change in the (111) peak in the XRD patterns of the CeO_2 NPs. The (111) peak is shifted toward a lower 2 theta value as the size of the CeO_2 NPs decreased. As the particle size d_{XRD} of CeO_2 decreased from 64.4 to 9.6 nm, the lattice parameter increased from 0.5406 to 0.5425 nm, a 3.5% increase (inset in Fig. 1). The lattice parameter of S-CeO_2 (0.5425 nm) was higher than that of bulk-CeO_2 (0.5403 nm) (JCPDS 65-5923), which is attributed to the increase of O vacancies with an increasing surface to volume ratio [19–21,23]. The formation of O vacancies left two free electrons on the Ce ions at the surface, leading to a reduction of Ce^{4+} to Ce^{3+}. This change in the oxidation state of the Ce ions leads to a lattice expansion of the CeO_2 structure (cubic fluorite) because the ionic radius of Ce^{3+} (1.143 Å) is bigger than that of Ce^{4+} (0.970 Å) [19].

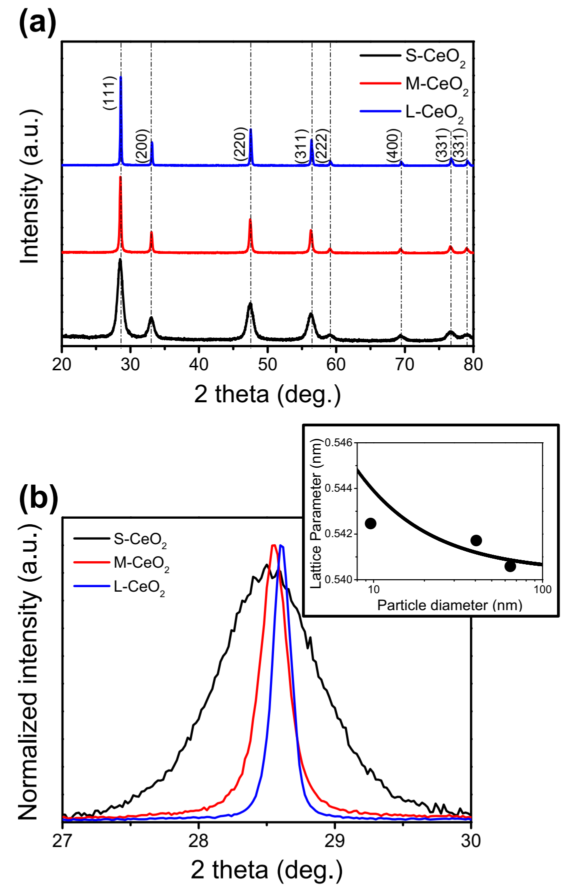

Fig. 1. (a) XRD patterns of CeO_2 NPs. (b) Magnified view of the (111) peak in XRD. The inset presents the lattice parameter of CeO_2 NPs as a function of particle size. The curve is obtained by the equation ($\alpha = \alpha_{bulk} + 0.036/D$) in ref 22.

The TEM images and fast Fourier transformed (FFT) patterns of the CeO_2 NPs are shown in Fig. 2. The size distributions of the CeO_2 NPs were measured from the TEM images (insets in Fig. 2). Both M-CeO_2 and L-CeO_2 NPs have a faceted shape whereas S-CeO_2 NPs have a rounded shape. The corresponding FFT patterns